HOSTED BY
ELSEVIER
Available online at www.sciencedirect.com
ScienceDirect
Soils and Foundations 66 (2026) 101807
www.elsevier.com/locate/sandf

Technical Paper

A method to determine contact parameters for particulate geomaterials: a guide to inter-particle experiments and their analysis

Saurabh Singh [a,b,*], Matthew Richard Coop [b], Beatrice Anne Baudet [b]

[a] School of Physics, Engineering, and Computer Science, University of Hertfordshire, UK
[b] Civil, Environmental and Geomatic Engineering, University College London, London, UK

Received 26 November 2025; received in revised form 14 May 2026; accepted 2 June 2026

Abstract

The prevalence of discrete element simulations necessitates a robust understanding of contact between granular particles. The inter-particle apparatus has been used in several past studies to characterise the contact behaviour of sands, ballasts, and rock particles. However, the problems related to compliance, out-of-plane forces, and resolution of true normal and tangential forces have not yet been completely solved. Most of these problems can be attributed to the unknown orientation of the plane of contact between two particles. This article describes methods to obtain accurate contact data by reducing compliance and provides analyses of various test stages. Additionally, an accurate contact normal is derived in tangential sliding, accounting for out-of-plane force and vertical-horizontal displacement profile. The closed-form solution for normal and tangential forces is also derived, along with contact traces on each particle. The efficacy of these solutions is presented through an example test on Leighton Buzzard sand.

Keywords: Inter-particle experiments; Compliance and corrections; Stiffness; Coefficient of friction

1. Introduction

Triaxial testing has played a pivotal role in the study of the macroscopic behaviour of soils through well-planned experiments (Roscoe et al., 1958; Verdugo and Ishihara, 1996). The experimental data led to important mathematical frameworks and constitutive models that were also calibrated using triaxial tests (Roscoe et al., 1963; Dafalias and Manzari, 2004). In recent times, advances in computational power have shifted the focus from a continuum approach to the particulate nature of soils through the discrete element method (DEM) (Cundall and Strack, 1979; Zhao et al., 2023). The early studies in DEM used circular or polygonal particles with simple contact behaviour (Iwashita and Oda, 1998; Mirghasemi et al., 1997). With time, significant advancements have been made in mimicking the particle shape and size distribution (Sun and Zheng, 2020; Zhao et al., 2023). DEM has witnessed significant development in simulating the behaviour of sands and other granular materials. However, very little attention has been given to the contact behaviour of granular particles. The contact parameters were either arbitrarily chosen or often determined by fitting one or a few triaxial tests (Cheng et al., 2018; Nguyen et al., 2025). The fitting exercise results in a non-unique set of parameters that may not reflect the inter-particle contact behaviour well. To tackle this problem, a modern version of the inter-particle apparatus and experiments has captured the interest of researchers, which may play the same role for DEM as triaxial tests in continuum modelling. It is likely that this type of testing will become a necessity if we continue to pursue particulate approaches.

* Corresponding author.
E-mail addresses: s.singh29@herts.ac.uk (S. Singh), m.coop@ucl.ac.uk (M.R. Coop), b.baudet@ucl.ac.uk (B.A. Baudet).

https://doi.org/10.1016/j.sandf.2026.101807
0038-0806/

Nomenclature

α	slope of vertical-horizontal displacement profile
δh	incremental horizontal displacement
δn	incremental normal displacement
δt	incremental tangential displacement
δv	incremental vertical displacement
δx_c	incremental displacement of the contact point along horizontal-1 direction
δx_t	incremental horizontal displacement of the base particle
δz_c	incremental displacement of the contact point along the vertical direction
δz_t	incremental vertical displacement of the top particle
θ	orientation of contact tangent along sliding direction
$f(x,y)$	surface of the top particle
$g(x,y)$	surface of the base particle
h_1	horizontal-1 displacement of the base particle
h_2	horizontal-2 displacement of the base particle
H_1	force on particles along the horizontal-1 direction
H_2	force on particles along the horizontal-2 direction
l_t	length of contact trace on the top particle
l_b	length of contact trace on the base particle
$\hat{n}$	unit normal vector on the contact plane
N	idealised normal force, $Vcos\alpha - H_1 sin\alpha$, in the absence of H_2 force
N	normal force at contact
R_{11}	radius of top particle from h_1 digital camera/microscope
R_{12}	radius of base particle from h_2 digital camera/microscope
R_1	mean radius (harmonic mean) of the top particle
R_{21}	radius of base particle from h_1 digital camera/microscope
R_{22}	radius of base particle from h_2 digital camera/microscope
R_2	mean radius (harmonic mean) of the base particle
R	effective radius of contact
$\hat{t}$	unit tangent vector along the sliding direction at the contact point
$\hat{t}_1$	unit tangent vector along the sliding direction at the contact point
$\hat{t}_2$	unit tangent vector normal to $\hat{n}$ and $\hat{t}_1$
T	tangential force at contact
v	vertical displacement of the top particle
V	vertical force acting on the particles at contact
(x_c, y_c, z_c)	contact point

A significant improvement has been made in the inter-particle testing in the last decade. The initial versions of inter-particle apparatuses had one or two arms (Skinner, 1969; Cole et al., 2010; Cavarretta et al., 2011; Senetakis and Coop, 2014), a vertical and a horizontal arm; the vertical arm was used to apply the vertical load at the contact, while the horizontal arm was used to move the base or top particle to study the effect of sliding. The control of actuators and resolution of transducers in vertical and horizontal directions were not good enough to measure small displacement stiffness or coefficient of friction after sliding due to unstable particle topography. These early apparatuses were also limited by their inability to measure the out-of-plane (of sliding) forces or displacements arising due to the complex topography of interacting particles (Singh et al., 2025). The orientation of the contact normal need not lie in this two-dimensional plane of vertical and horizontal arms, which implies that any resolution of horizontal and vertical forces, obtained with this two-dimensional apparatus, will not give the true contact normal force. A third arm was added by Nardelli and Coop (Nardelli, 2017; Nardelli and Coop, 2019) to measure out-of-plane effects and to avoid any out-of-plane force/displacement. Regular particles were chosen in the experiments, as it was not clear how to resolve the forces for a complex topographical surface with an unknown contact normal.

Particle- and mesoscale features give rise to the complex behaviour of granular materials (Iwashita and Oda, 1998). To understand the macroscopic behaviour, the mineralogical and topographical characterisation of individual particles is often carried out. The shape distribution of granular particles has long been studied using imaging methods to characterise form, roundness, and roughness of particles (Wadell, 1932; Barrett, 1980; Zheng and Hryciw, 2015). The effect of shape on macroscopic behaviour has been of interest to many researchers in the past few decades (Santamarina and Cascante, 1998; Shin and Santamarina, 2013). In particle-scale tests, the radius of curvature at contact has been a key parameter along with surface roughness. A high-degree polynomial or a high-pass filter is used to obtain the rough surface from the overall shape (Altuhafi et al., 2024). The power spectral density approaches have also been shown to be very effective in the study of fractal natural granular particles (Persson et al., 2004; Yang et al., 2016).

In this article, several developments in the procedure and analysis of inter-particle testing have been reported to help obtain accurate contact behaviour. These are listed in the following:

- A new inter-particle apparatus was designed specifically to address the compliance of existing apparatus. The normal compliance of the Nardelli (2017) apparatus was 0.61 μm/N (stiffness – 1.652 N/μm); whereas our apparatus has a normal compliance of 0.02 μm/N (stiffness – 50 N/μm) as shown in the Fig. 3. This compliance, or apparatus deformation, is calibrated and then subtracted from the measured displacements during a test, but when the correction is large the accuracy of the corrected displacement can be compromised.
- In addition, we have installed our displacement transducers on the top and base platen instead of the sled or horizontal arms. This removes some components of the apparatus from contributing to the compliance thereby increasing the accuracy of horizontal and vertical displacements in various stages of the tests. Further, the vertical arm is provided intermediate support through a bearing block where four sets of orthogonal linear bearings ensure only vertical motion of the arm while preventing any horizontal fluctuations.
- An improved method of preparing the sand sample in which the particles are ground flat at one end to reduce further the compliance associated with particle-platen contact. In prior studies, a nonconforming contact between platen and particle resulted in extra compliance that may have influenced the stiffness data.
- A standardised procedure for different testing stages is proposed along with microscopic scans for the initial and deformed surface of sand particle. This procedure also describes the physically informed choices for the rate of loading in various stages taking into account of their expected contact stiffness.
- An analytical relation between the profile of particles and their contact trajectory has been missing in the literature. This article investigates the relation between generic three-dimensional profiles of particles, the motion of the contact point, and contact traces on each particle during relative sliding of particles.
- The resolution of contact forces is studied in the setting of the inter-particle apparatus and its testing procedure. Prior studies ignore the out-of-plane forces and assume that the contact normal lies in the plane of sliding. Taking into account of displacement and force data including the out-of-plane force, analytical expressions are derived for normal and tangential loads in different stages of inter-particle testing.
- Existing assumptions and the validity of the analytical expressions are also addressed in this article.

With the developments presented in this article, it is possible to test particles with randomly complex surface topography and avoid the statistical bias of choosing only regular surface particles, as has typically been done in the past (e.g. Nardelli and Coop, 2019).

2. Apparatus and calibrations

The most commonly used inter-particle apparatus contains two arms – a vertical arm for loading the particle from the top and a horizontal arm for relative displacement of the top particle with respect to the base particle. The surface topography of natural granular particles renders this setup incomplete. In a two-arm setup, it is often assumed that the out-of-plane direction is parallel to the contact plane. This is not true due to the irregular nature of the granular particles. An inclination of the contact plane with the out-of-plane direction results in a component of normal force along the out-of-plane direction. This out-of-plane direction force is not measured if the third arm is not present. An additional arm addresses these issues and also facilitates more nuanced tests.

Fig. 1 presents the details of the inter-particle apparatus designed at University College London (UCL) for testing small-sized particles (1–2 mm). This inter-particle apparatus has three arms – two arms in the horizontal plane and one vertical arm. Each arm is equipped with a linear actuator (i in Fig. 1a), a load cell (iv in Fig. 1a), and a capacitive displacement transducer. The three linear actuators are housed in a block, fixed on the stiff platform, which reduces the compliance of the actuator nose. The load cell and actuator are screwed into a connecting block (iii in Fig. 1a). A linear bearing is placed underneath this connecting block (Fig. 1c) to allow linear motion without any additional frictional force or moments. The independent movement of the sled in the horizontal plane is facilitated by the guide rail and linear bearing assembly (Fig. 1b), along with the support of ball bearings (Fig. 1c). The ball bearings minimise the friction in relative movement and provide adequate mechanical support to the sled. Additionally, it is ensured that the loading axes along vertical and horizontal directions pass through the contact plane of the two particles to minimise additional indeterminate moments at the contact. The following subsection describes the procedures that should be followed, independent of the design of the inter-particle apparatus.

2.1. Calibration of the sensors and transducers

The desired precision of sensors and transducers in an inter-particle apparatus is very high due to the high stiffness of contact. Natural granular particles deform only a few microns for a few Newtons of contact load (typically 1 μm to 20 μm in 1 N to 50 N – Nardelli, 2017; Nardelli and Coop, 2019; Wong and Coop, 2023). As in an assembly of sand particles, the contact forces in strong force chains can be even smaller and hence further high resolution of displacement and loads is required. A common concern in using such high-resolution sensors and transducers is the change in calibration due to fatigue (structural

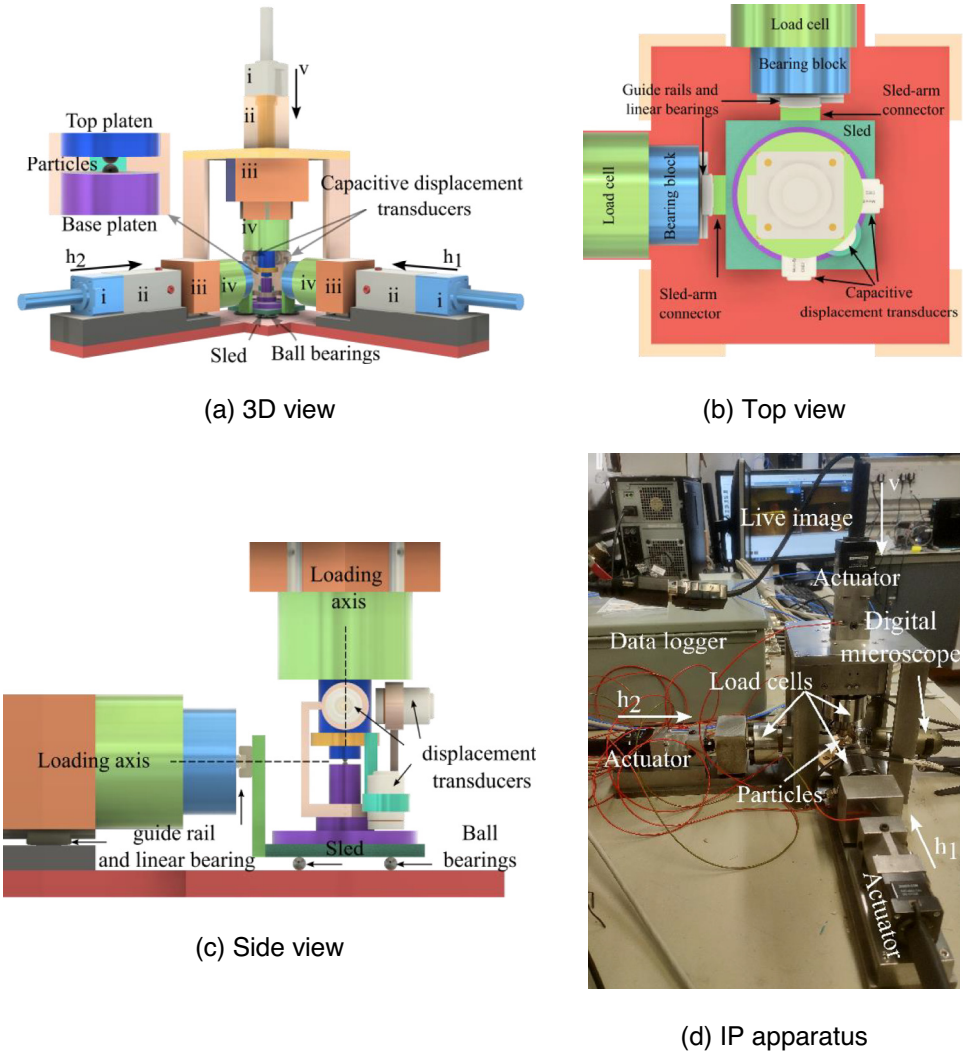

Fig. 1. Compact design of the new inter-particle apparatus at UCL. (a) 3D view of the interparticle apparatus (labels: i – linear actuator, ii – actuator housing block, iii – load cell and actuator connection, iv – load cell); (b) top view of the apparatus – showing the configuration of guide rails and bearing blocks; (c) side view of the apparatus – role of ball bearings and loading axes; (d) actual inter-particle apparatus developed for testing small granular particles.

degradation of sensors due to repeated loading–unloading cycles over time) or electronic reasons. In the inter-particle apparatus, a frequent calibration of these transducers and sensors is performed to keep the measurements effective (Cavarretta et al., 2011; Nardelli, 2017; Wong, 2022). A detailed example of calibration of load cells and transducers is provided in Appendix A.

2.2. Compliance tests

Fig. 2 shows a spring-dashpot-slider model for the inter-particle apparatus. The normal and tangential stiffness at a particle contact can be affected by the stiffnesses of the vertical and horizontal arms. If the measurement of displacement includes a compliant part of the apparatus, a compliance correction must be performed. Also, the mechanical systems of an inter-particle apparatus may become unstable if the stiffnesses of the horizontal and vertical arms are low. To avoid these problems, a compact and robust inter-particle apparatus is designed with stiff connections while facilitating the desired motion of its members.

The contact stiffness of natural granular particles is up to 5 N/μm (Wong, 2022). The vertical and horizontal arms of an inter-particle apparatus should have significantly higher stiffnesses. Fig. 3 shows a typical test which can be performed for the calibration of apparatus compliance (Nardelli, 2017; Wong, 2022). To measure the vertical compliance, a steel block is placed between the top and base platen and compressed to obtain the load–displacement behaviour within the measurement system (Fig. 3a). The stiffness of the apparatus was obtained to be 50 N/μm (50000 N/mm), which should suffice for measurements within the range of 25 N. A similar test can also be performed for horizontal compliance by gluing the steel block; the glue should be cured under normal load to minimise its

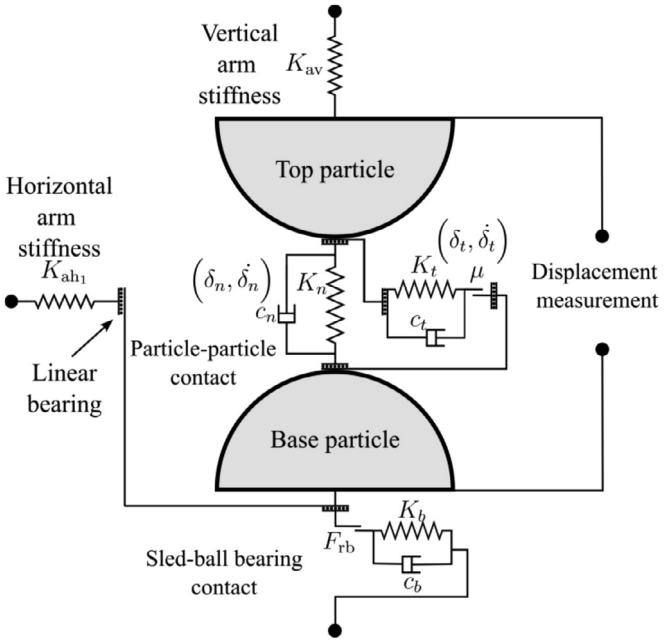

Fig. 2. Spring-dashpot-slider model for particle–particle contact and apparatus compliance (labels: K_* – stiffness of the different components, c_* – damping coefficient, μ – coefficient of friction, F_{rb} – rolling friction force).

thickness. In actual experiments on the shearing behaviour of sands, the relative movement of the particles at the contact is achieved by gluing the particles to the platen. This calibration with the glued steel block is a calibration of the compliance of the apparatus and the glued interface.

Hertz (1881) developed the theory of contact between spherical bodies. The efficacy of our apparatus is also shown in Fig. 3b, which shows that the measured load–displacement behaviour of the steel ball (Young's modulus – 210 GPa and Poisson's ratio – 0.3) matches well with the Hertz prediction.

2.3. Calibration of the sled-ball bearing system for frictional sliding

An important aspect of inter-particle tests is to measure the tangential stiffness and coefficient of friction at the particle–particle contact. In Fig. 2, the tangential response of the particle–particle contact is affected by the sled-ball bearing contact at the base (Nardelli, 2017; Wong, 2022). Forces measured on horizontal load cells include forces due to the sled-ball bearing contact, and these forces must be taken into account for the measurement of the coefficient of friction and tangential stiffness. The horizontal loads are also affected by any misalignment of the guide rail and linear bearing assembly, particularly due to an inclination between their orientation planes (Fig. 1b). It is quite easy to get such a misalignment if appropriate precautions are not observed during the experiments. To avoid errors due to these factors, the friction due to sled and other sources is calibrated at the start of each test.

Fig. 4a shows the horizontal force applied to displace the sled while the top particle is not in contact with the base particle. This force is a resultant of sled friction and misalignment between linear bearings. Before each experiment, sled calibration is performed to ensure that this force is significantly lower than the expected contact frictional force. Furthermore, if the forces are set to zero before different stages of loading, the sled friction force may shift its origin to a positive or negative load depending on the previous direction of horizontal loading. This shift is calibrated through cyclic movement of the sled without particles in contact, as shown in Fig. 4b.

3. Characterisation of surfaces and profile curvatures

The contact behaviour of natural particulate geomaterials depends on the local topography of the surface. These

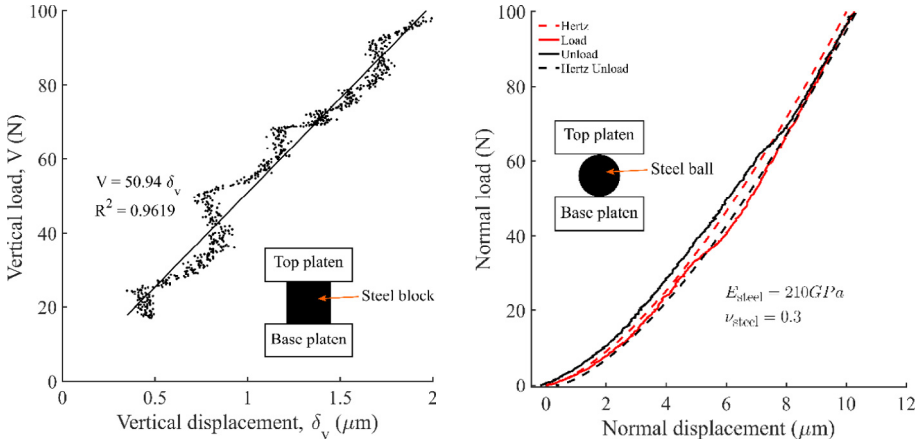

(a) Compliance of the vertical arm with the steel block

(b) Compliance of the vertical arm with the steel ball

Fig. 3. Compliance correction for the vertical arm. (a) With a steel block; (b) with a steel ball.

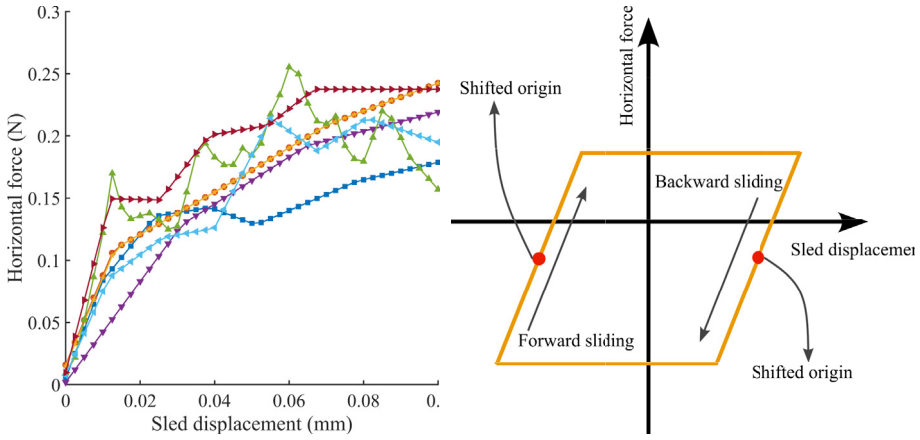

(a) Sled friction force (b) Shifted origin in cyclic loading

Fig. 4. Frictional force on the sled due to ball bearings. (a) Sled frictional forces; (b) shifted origin of sled friction due to incorrect offset.

surfaces are self-affine at several scales, characterised by the roughness parameters such as root mean square roughness, root mean square slope, Hurst exponent or fractal dimension (Yang et al., 2016). The fractal nature of surfaces renders the real contact area significantly smaller than the apparent contact area, in turn making it much softer than a smooth elastic contact. There is increasing evidence that suggests that the coefficient of friction of natural particulate geomaterials depends on the surface roughness (Nardelli and Coop, 2019). In characterising the roughness, the mesoscale shape features make the extraction of the roughness component of the surface challenging. A couple of methods, relying on fitting the overall shape of the particle, have been used to obtain the roughness component (Boulanger, 1992; Otsubo and O'Sullivan, 2018; Li et al., 2021). The power spectral density-based approach of characterising the surface reduces the subjectivity of choosing different parameters (Persson et al., 2004; Yang et al., 2016); however, some choices have to be made regarding the structure function to relate the fractal dimension and Hurst exponent.

The particles, before experiments, are scanned with a high-resolution surface microscope such as an optical stereoscope (for ballast-sized particles), a laser confocal microscope (for a range of sand and ballast-sized particles), and optical interferometry (for opaque, relatively smooth sand particles). A three-in-one Keyence microscope with optical microscopy, laser confocal microscopy, and optical interferometry is used for characterisation of the surfaces of natural granular particles, as shown in Fig. 5a. Fig. 5b shows a typical surface of a coral sand particle obtained using laser confocal microscopy, which is quite challenging to obtain using interferometry and loses significant resolution in optical stereoscopy.

In Hertz contact theory, for smooth elastic bodies in contact, the deformation in the contact region depends on the effective radius of curvature and the elastic properties of the contacting bodies. The effective radii of curvatures can be obtained using the surface scans of the top and the base particles. In the absence of the surface microscopes, the digital microscopes (Fig. 1d) are used to obtain the images of contacting bodies, as shown in Fig. 6. The resolution provided by the digital microscopes is not high enough to calculate roughness, but it is sufficient for the radius of curvatures. To calculate the effective radius of curvature, the profile of particles (shown in green in Fig. 6) is extracted using image analysis or manually for two orthogonal directions, h_1 and h_2. The radii of curva-

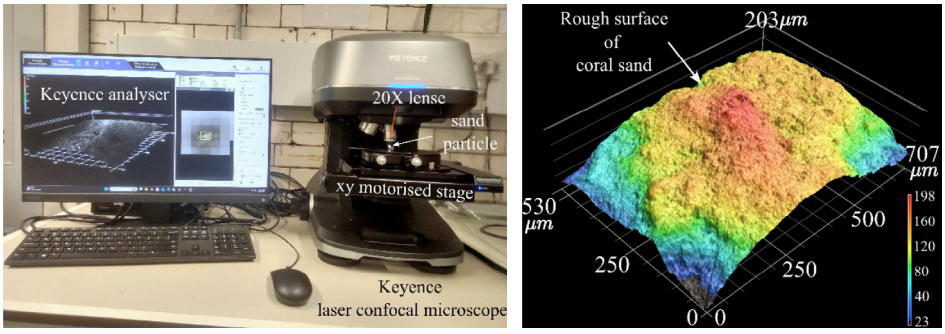

(a) Keyence laser confocal microscope (b) Rough surface of coral sand

Fig. 5. Surface characterisation of particles.

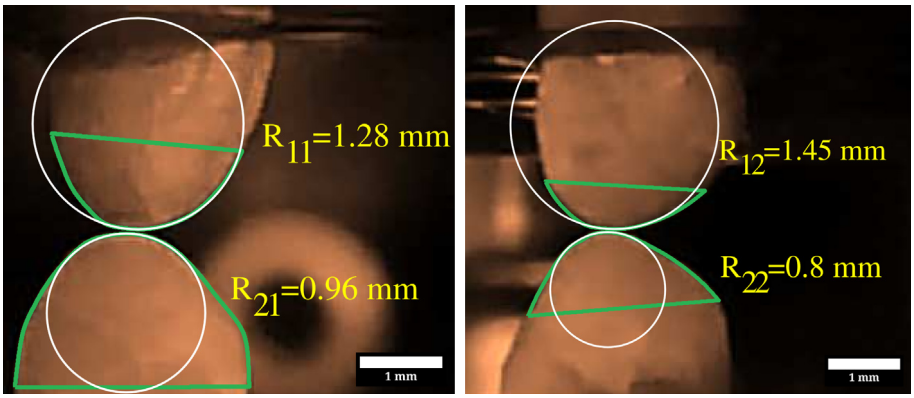

(a) h_1-direction image (b) h_2-direction image

Fig. 6. Curvature estimation for the top and base particle. The radius of curvature is calculated using the profiles of particles near the contact region along two orthogonal directions: (a) h_1 and (b) h_2.

tures (top particle: R_{11} and R_{12}, and base particle: R_{21} and R_{22}) are calculated by fitting a parabola near the contact point. The harmonic mean of radii along h_1 and h_2 directions gives the mean radius of curvature (R_1 and R_2). From the mean radius of curvature, the effective radius of contact, required by Hertz theory, is calculated by $1/R = 1/R_1 + 1/R_2$.

4. Analysis of particle–particle experiments

There are only a few studies in the literature that include particle–particle experiments (Skinner, 1969; Cole et al., 2010; Cavaretta et al., 2011; Senetakis and Coop, 2015; Altuhafi et al., 2024; Nardelli, 2017; Sandeep et al., 2018; Nardelli and Coop, 2019; Wong and Coop, 2023). These experimental studies include at most four stages to obtain the inter-particle contact behaviour in normal and tangential directions: establishing contact between particles, vertical loading to the desired normal load, horizontal loading to the desired shear displacement, and cyclic loading. This sequence allows the non-linear normal and tangential stiffnesses to be measured on the same particles. Typically, the tests are monotonic with tangential loading at the maximum normal load applied. This is because any history of prior normal loading to higher loads or pre-shearing will affect the measured response (see e.g. Nardelli & Coop, 2019). The final stage of large displacement cycling is not essential and only checks for modification of the inter-particle friction due to contact wear. The following subsections describe these stages and their analysis in detail.

4.1. Preparation of the experiment

In previous experimental studies, the particles in their natural shape were glued in a cylindrical groove with epoxy or superglue (Senetakis et al., 2013; Senetakis and Coop, 2015; Sandeep et al., 2018; Nardelli, 2017; Nardelli and Coop, 2019), as shown in Fig. 7a. With such an arrangement, there exist two compliant particle-platen interfaces, which result in additional displacement and lower apparent stiffness of the particle–particle contact, introducing inaccuracy in the measurement. Alternatively, to avoid compliant interfaces, particles can be ground flat and then glued to the platens as shown in Fig. 7b. A fixture was designed to apply a seating load on the ground particles to create a flat particle-platen interface, as shown in Fig. 8. The seating load reduces the glue thickness underneath the particle. The fixture also centres the particle and protects the contact region from the seating load. The glued interface, with seating load, is left to cure for 15–18 h. Particles, mounted on the platen, are washed and dried for surface scanning.

4.2. Establishing contact

After scanning the particles, the platens are screwed into the apparatus. The apexes of the top and base particles are aligned to minimise out-of-plane forces. The live images on the digital microscope ensure alignment accuracy. If one of the particles is flat, the apex of the other particle is moved to the scanned area of the flat particle. During alignment, the particles are kept separated by a few millimetres. At this stage, a sled calibration is performed to reset the origin of horizontal load and to check the frictional forces on the sled. The pictures along orthogonal planes (h_1-v and h_2-v) are captured using the digital microscope to calculate the curvatures.

Before establishing contact, the top particle is brought close to the base particle in a manual control mode. The actuator speed is gradually decreased in steps – from 0.1 mm/s to 0.01 mm/s, and finally to 0.001 mm/s – to close the initial gap of a few millimetres between the particles. A computer control mode is set up once the gap becomes indiscernible in the digital microscope's live image. In this mode, the vertical arm moves downward at a rate of 50 μm/hour with the computer controlling the movement every 10 s, resulting in a 0.14 μm increment per step. If the initial stiffness of the contact is, say, 1 N/μm (it is often less than 1 N/μm for sand and ballast particles), the load at

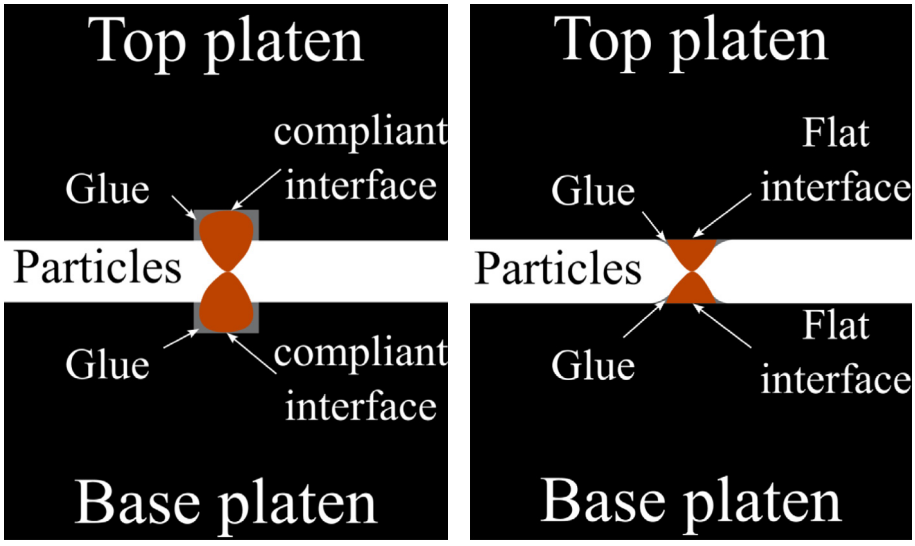

(a) Complete particle (b) Ground flat particle

Fig. 7. Reducing the compliance of non-particle–particle components. (a) Using a full particle in a groove with glue; (b) using a flat ground particle with glue (cured under weight).

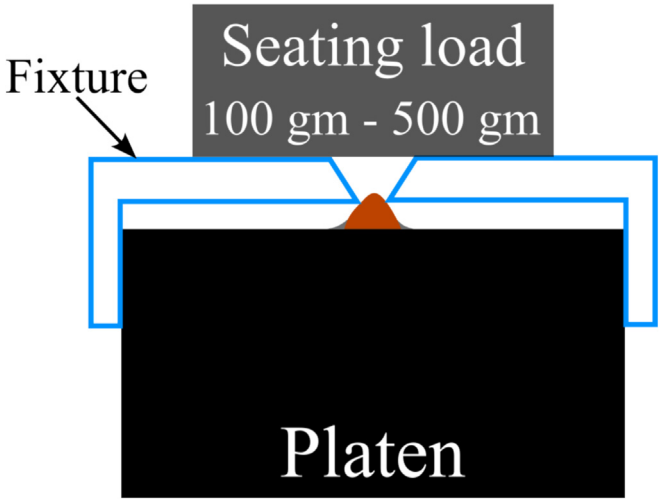

Fig. 8. Curing of the glued interface between particle and platen.

first contact would be at most 0.14 N. At this stage, loading can either continue in displacement control mode or be switched to load control mode.

For ballast or rock particles, the gap between the particles is often not clearly visible in the digital microscopes due to their complex topography. The gap could be a few millimetres and still indiscernible in the microscope. A computer control mode at this stage may take a few hours to establish contact. A higher load at initial contact is admissible for these particles as they are often subjected to significantly high loads. The top particle is moved downward at a rate of 500 μm/h or higher in this case. With a computer control interval of 10 s, the displacement increases 1.40 μm per step. The load at first contact would be at most 1.40 N. After the first contact, the loading is switched to load control mode for rock or ballast particles.

4.3. Loading stages

As described in the previous section, after establishing contact, the vertical loading is continued either under displacement control or load control mode. The normal contact between natural granular particles becomes stiffer with deformation as the normal stiffness increases as a power law with deformation (Hertz, 1881). At small deformations, a small increment in displacement results in a small increase in the normal force, but at large deformations, a small increment in displacement results in a large increase in the normal force. If the particle is loaded to a small deformation or a small load, the displacement control mode is a quick and reliable choice. However, if the particles are loaded to large deformations or large loads, a load control mode is a better choice to obtain sufficient data points for the accurate measurement of stiffness. For sand particles, loaded to small loads, a displacement rate of 0.05 mm per hour was found suitable. Caution must be taken while testing particles with large radii of curvature, as in such cases, it may be suitable to further reduce the displacement rate. For ballast particles, after establishing contact with the displacement control mode, the loading is switched to load control at a rate of 50–200 N per hour.

Even when care is taken to keep the contact apex to apex (with zero slope along both h_1 and h_2 directions), the slope of the initial contact may be non-zero for irregularly shaped natural particles. The inclination of the contact plane may result in a tendency for horizontal movement of the sled when the vertical arm is moved downwards. The inter-particle testing apparatus must therefore have both horizontal arms to prevent unintended horizontal movements and to measure the loads required to do so. In vertical loading, the horizontal arms are kept

at rest. However, as the horizontal loads increase due to the non-zero slope of the contact, a small horizontal displacement (often less than a few microns) is observed. The horizontal forces are generally quite small in comparison to the vertical force, and when the normal force is resolved, the normal force is quite close to the vertical force. While the normal load behaviour is obtained with quite good accuracy, there is therefore some mobilisation of tangential force that may happen during vertical loading.

At the end of the vertical loading stage, it is recommended to perform an unload-reload cycle to obtain the elastic normal stiffness before starting tangential shearing, since most of the displacement during the first normal loading is typically irrecoverable. Also, the data is enriched if the surface scans are performed at this stage to evaluate the change in the roughness; however, this is not always feasible. During normal loading, the curvature of particles will change at the contact region, but this is too small to observe with the digital microscope. As highlighted earlier, the contact point between the two particles must pass through (or within an acceptable tolerance) the horizontal and vertical loading axes. A significant misalignment will generate a moment at the contact region, and the distribution of surface traction will be affected, in turn affecting the contact stiffnesses.

In tangential shearing, the base particle is moved relative to the top particle, usually in displacement control mode, while keeping the vertical load constant. To keep contact between particles at a constant vertical load, the top particle moves vertically according to the profile of both particles. The out-of-plane-of-shearing direction is kept fixed, and reactions on that arm are measured. The shearing arm is moved at a displacement rate that facilitates recording of the reduction in tangential stiffness and the onset of tangential sliding. A displacement rate of 0.05 mm per hour has been found suitable for most sand particles and 0.1 mm per hour for ballast particles or rock fill. The displacement rate in sliding can be increased further; however, it is limited by inertial effects in the control systems. If the height of the ground particle is significantly large in comparison to its base, it may cause a significant moment at the platen-particle interface, resulting in rupture of the bonded interface and failure of the experiment. At the start of tangential shearing, it is recommended to perform pre-sliding cycles to gauge the component of elastic and plastic mobilisation of deformation.

4.4. Assumptions and setting for analysis

In the vertical loading, the sand particles deform under normal compression over a contact region. This contact region may consist of several subregions between different sets of asperities within the overall contact region. Each subregion may have its own contact normal. It is assumed that the contact happens over only one region with a unique contact normal that may also be construed as an equivalent contact region in the case of several contact subregions. In tangential loading, this analysis only considers sliding along one of the horizontal (h_1 or h_2) axes while keeping the other fixed. For sliding along a more general path, a moving coordinate system can be considered such that the incremental sliding happens in one of three orthogonal coordinate planes. However, for the purpose of inter-particle tests, this general path sliding is not required to obtain the contact behaviour.

Further, it is assumed that the tangential friction force along a certain direction only mobilises with non-zero displacement along that direction. For example, if sliding occurs on v-h_1 plane while keeping h_2 fixed (no displacement along h_2) then no tangential friction force mobilises along t_2-axis (out-of-plane-of-sliding contact tangent axis) as displacement along t_2-axis is zero. In addition, it is also assumed that the normal deformation of the particles is not affected by sliding, which is only valid if the normal load and effective radius of curvature do not change in sliding.

The analysis in subsequent sections is performed on the forces corrected for sled friction and displacements corrected for compliance.

4.5. Profile of particles and orientation of contact

Fig. 9 shows schematics of the particle–particle interaction during tangential sliding. The top particle moves vertically downward along the positive z-axis (v-axis), and the base particle is moved in the horizontal plane along the positive x-axis (h_1-axis). The displacements are assumed positive along the positive x- and z-axes. Fig. 9a, c show the initial contact between particles with the contact plane at point (x_c, z_c), and Fig. 9b, d show the relative shearing of particles where the top particle moves downward, and the base particle moves forward while keeping the contact intact. In the following, a relation for the orientation of the contact is derived in the form of incremental vertical displacement and incremental horizontal displacement. The surfaces of the top particle and base particle are denoted by $z = f(x,y)$ and $z = g(x,y)$, respectively. In the Fig. 9, only the cross-section of the sliding $(z - x)$ is shown.

In general, for two smooth particles forming a non-conforming contact, the following conditions are always true:

- **Contact condition**: Both particles, i.e. their boundary surfaces, touch at the point of contact (see Fig. 9)

$$z_c = f(x_c, y_c) = g(x_c, y_c) \tag{1}$$

- **Non-overlap condition**: At the point of contact, the slopes of top and base particles are the same (Eq. (2)), which is also the slope of contact (see Fig. 9). If that is not the case, the particles will overlap or intersect.

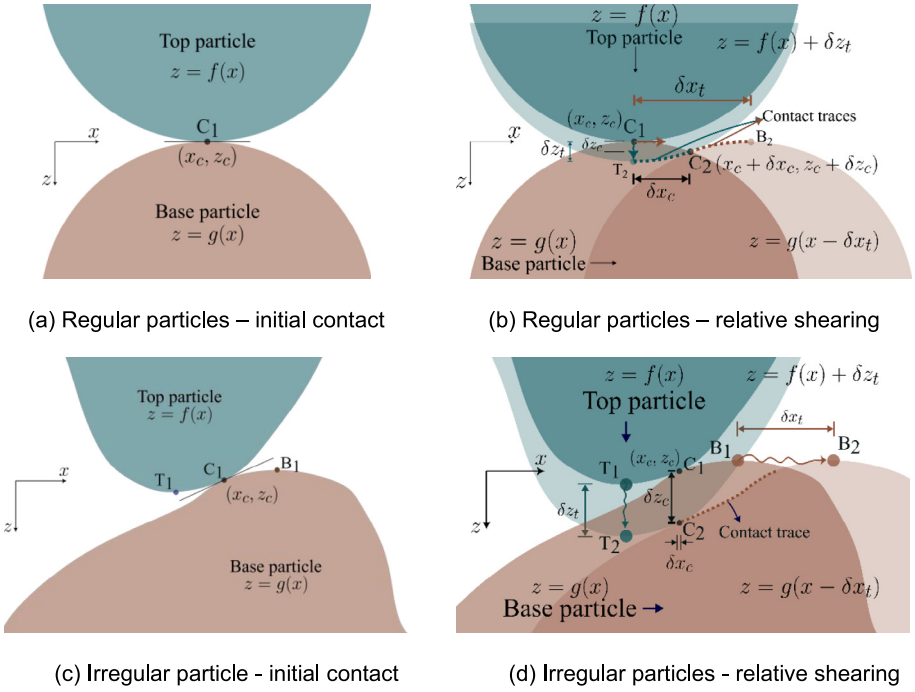

Fig. 9. Orientation of contact in the relative motion of particles in tangential shearing. (a), (c) initial contact; (b), (d) relative shearing. The top particle moves only in the vertical (z) direction, whereas the base particle moves only in the horizontal (x) direction.

$$\left.\frac{\partial z}{\partial x}\right|_{(x_c,y_c)} = \left.\frac{\partial f}{\partial x}\right|_{(x_c,y_c)} = \left.\frac{\partial g}{\partial x}\right|_{(x_c,y_c)} \quad \text{(a)}$$
$$\left.\frac{\partial z}{\partial y}\right|_{(x_c,y_c)} = \left.\frac{\partial f}{\partial y}\right|_{(x_c,y_c)} = \left.\frac{\partial g}{\partial y}\right|_{(x_c,y_c)} \quad \text{(b)} \qquad (2)$$

In the tangential sliding, the base particle is moved by a small displacement δx_t under a constant vertical load (the updated surface of the base particle is then – $z = \widetilde{g}(x,y) = g(x - \delta x_t, y)$). To keep the vertical load constant, the top particle moves vertically downward by δz_t (the updated surface of the top particle is – $z = \widetilde{f}(x,y) = f(x,y) + \delta z_t$). In this process of infinitesimal sliding, the displacement of the contact point is $(\delta x_c, \delta z_c)$, i.e., the new contact point becomes $(x_c + \delta x_c, z_c + \delta z_c)$. For this new contact, the above conditions, contact and non-overlap, are still true. Using the first condition,

$$z_c + \delta z_c = \widetilde{f}(x_c + \delta x_c, y_c) = \widetilde{g}(x_c + \delta x_c, y_c)$$
$$z_c + \delta z_c = f(x_c + \delta x_c, y_c) + \delta z_t = g(x_c + \delta x_c - \delta x_t, y_c) \qquad (3)$$

Now, substituting z_c from Eq. (1) in Eq. (3) and using the Eq. (2a), slope of contact tangent in the plane of sliding is:

$$\left.\frac{\partial g}{\partial x}\right|_{x_c,y_c} = \left.\frac{\partial \mathrm{f}}{\partial x}\right|_{x_c,y_c} = -\frac{\delta z_t}{\delta x_t} \qquad (4)$$

The incremental vertical displacement of the top particle (δz_t) and incremental horizontal displacement of the base particle (δx_t) are enough to obtain the slope of contact along the direction of sliding.

Using the second condition,

$$\left.\frac{\partial \widetilde{f}}{\partial x}\right|_{(x_c+\delta x_c,y_c)} = \left.\frac{\partial \widetilde{g}}{\partial x}\right|_{(x_c+\delta x_c,y_c)} \qquad (5)$$

Further, using Eqs. (2) and (5), incremental displacement of the contact point is:

$$\delta x_c = \frac{\left.\frac{\partial^2 g}{\partial x^2}\right|_{(x_c,y_c)} \delta x_t}{\left.\frac{\partial^2 g}{\partial x^2}\right|_{(x_c,y_c)} - \left.\frac{\partial^2 f}{\partial x^2}\right|_{(x_c,y_c)}}$$
$$\delta z_c = \frac{\left.\frac{\partial g}{\partial x}\right|_{(x_c,y_c)} \left.\frac{\partial^2 f}{\partial x^2}\right|_{(x_c,y_c)} \delta x_t}{\left.\frac{\partial^2 g}{\partial x^2}\right|_{(x_c,y_c)} - \left.\frac{\partial^2 f}{\partial x^2}\right|_{(x_c,y_c)}} \qquad (6)$$

Fig. 9 shows the traces of contact points for the top and base particles, l_t and l_b, respectively. These traces can be obtained using the following relations:

$$l_t = \int_{x_c}^{x_c + \delta x_c} \sqrt{f_x^2 + 1}\, dx$$
$$l_b = \int_{x_c}^{x_c + \delta x_c - \delta x_t} \sqrt{g_x^2 + 1}\, dx \qquad (7)$$

The lengths of the contact traces are different for base and top particles. This implies that the top and base particles may undergo different amounts of material tangential sliding due to their surface complexities.

Fig. 10 shows initial contact and its evolution in tangential shearing for regular and irregular particles. The initial reference configurations are shown in dashed lines. The traces of the contacts are shown by dots on the particle outline. Note that the contact traces are not of identical length

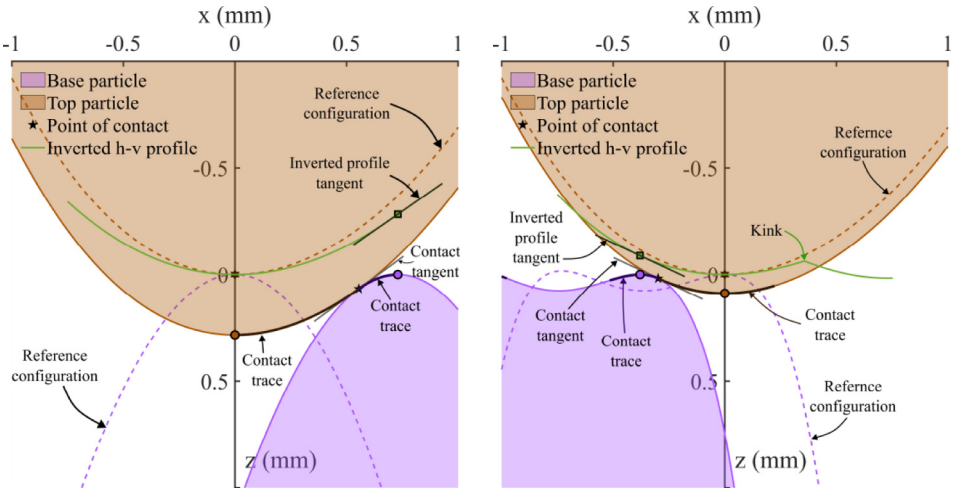

Fig. 10. Relationship between contact tangent and slope of inverted profile. (a) For regular particles; (b) irregular particles.

for top and base particles, i.e., both particles undergo different amounts of sliding. The contact traces for the top and base particles are dependent on the form of the particles as given by Eq. (7). To study the frictional sliding between natural sand particles, it is desirable to obtain a similar geometrical form for both particles across the suite of experiments to get similar contact traces. However, this requirement is quite stringent, and it is nearly impossible to test pairs of sand grains which have similar curvature. The primary difficulty arises from the small size of sand particles and grinding them flat to place them on platens. Along with contact traces, Fig. 10 also shows the recorded displacement profile (inverted h-v profile, inverted due to minus sign in Eq. (4)) between horizontal and vertical displacement. Eq. (4) suggests that the slope of the inverted profile (h vs –v) is equal to the slope of the contact. Fig. 10 shows that the tangent of the inverted profile is parallel to the contact tangent. Fig. 10b shows that the h-v profile may not be differentiable at all points, even though the form of both particles may be smooth and continuous. If such a case is encountered in the experiments, profile-slopes must be calculated in piece-wise manner prior to any non-differentiable point and after it. The point of non-differentiability should be ignored in the analysis. The supplementary material contains some example videos to illustrate these concepts.

4.6. Analysis of vertical loading

Fig. 11 shows the deformation of the particles in vertical loading as the top particle is moved downward and the base particle is kept fixed. The semi-transparent solid lines show the reference configurations of the particles with an initial contact. The deformed configuration is shown in solid lines, while the dashed outline of the top particle shows the translated reference configuration. The inclination of the vertical load with normal to the contact results

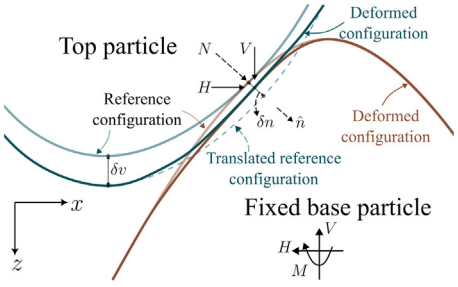

Fig. 11. Resolution of forces in vertical loading – the top particle moves downward while the base particle remains fixed.

in both normal and tangential deformation. As the top particle is moved downward with an incremental displacement $\delta v\hat{e}_3$, the top and base particles deform δn_1 and δn_2 respectively along the contact normal, and result in a net deformation of the contact by $\delta n\hat{n}$. A component of incremental vertical displacement ($\delta v\hat{e}_3 = \delta n\hat{n} + \delta t\hat{t}$) results in tangential displacement $\delta t\hat{t}$ which may cause mobilisation of tangential force during the vertical loading stage. The forces can be simply resolved as:

$$N = V(\hat{e}_3 \cdot \hat{n}) + H_1(\hat{e}_1 \cdot \hat{n}) + H_2(\hat{e}_2 \cdot \hat{n})$$
$$T = \sqrt{H_1^2 + H_2^2 + V^2 - N^2} \tag{8}$$

The normal and tangential forces cannot be resolved as $\hat{n}$ is unknown. Assuming frictional force mobilises only insignificantly ($\delta t \approx 0$) will lead to $N = \sqrt{V^2 + H_1^2 + H_2^2}$, $\hat{n} = \frac{H_1\hat{e}_1 + H_2\hat{e}_2 + V\hat{e}_3}{N}$, $\delta n = \delta v \frac{V}{N}$ and zero tangential force. With the current setup, there appears to be no way to obtain the orientation of contact in vertical loading under general setting. To minimise the error due to an inclination of the contact normal and vertical load, the contact should either be an apex-to-flat contact or an apex-to-apex contact, which can be confirmed by the small magnitudes of H_1 and H_2.

If H_1 and H_2 are significant, the contact normal can only be estimated from the orientation of the deformed contact region by scanning one of the particles.

4.7. Resolution of normal and tangential forces and displacements during sliding

Fig. 12 shows the forces acting on the base particle (in the x-z plane) as it slides forward along the positive x-direction while the top particle applies a constant vertical load. In the region of contact, the base particle is subjected to a normal force (N) and a tangential force (T), which are applied and measured along horizontal (force H_1 and H_2) and vertical (V) directions. The relative tangential displacement of the particles is reflected in the changes in horizontal (h_1, h_2) and vertical (v) displacements. Even if the contact normal aligns with the vertical load in the vertical loading stage, it is not possible to ensure the same during sliding, as the apex of the base particle will slide off the apex of the top particle. In tangential shearing, it is possible to evaluate the contact orientation at each point of contact. To avoid complexities in regard to the orientation of contact, the base particle is moved only along the h_1 or h_2 direction. Fig. 12 only shows an increment of the motion during tangential sliding with incremental displacement ($\delta z_t = \delta v$ and $\delta x_t = \delta h_1$) of top and base particles. Using Eq. (4), the orientation of contact (θ) and unit tangent vector ($\hat{t}$) can be calculated, i.e.,

$$\begin{aligned} tan\theta &= \frac{\partial g}{\partial x} = -\frac{\delta z_t}{\delta x_t} = -\frac{\delta v}{\delta h_1} = -tan\alpha \\ \hat{t} &= cos\theta\hat{e}_1 + sin\theta\hat{e}_3 = cos\alpha\hat{e}_1 - sin\alpha\hat{e}_3 \end{aligned} \tag{9}$$

The angle α is the slope of vertical vs horizontal displacement plot. The normal to the surface on the region of contact is unknown, and, hence, the normal force (N) is unknown (Fig. 12 shows the force perpendicular to the contact slope in the x-z plane as $\bar{N}$ which, in general, is not equal to N). Taking a general form of a unit normal

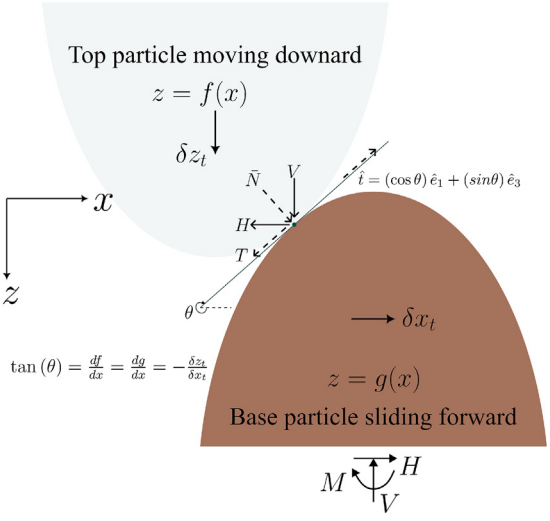

Fig. 12. Resolution of forces in tangential sliding.

to the surface at the contact point as $\hat{n} = n_1\hat{e}_1 + n_2\hat{e}_2 + n_3\hat{e}_3$ and using the orthogonality with the tangent vector ($\hat{t}$), it is easy to show that

$$\hat{n} = n_3 tan\alpha\hat{e}_1 \pm \sqrt{1 - n_3^2 sec^2\alpha}\hat{e}_2 + n_3\hat{e}_3 \tag{10}$$

From Fig. 12, the force acting on the region of contact on the base particle can be written as:

$$\vec{F} = N\hat{n} - T\hat{t} = V\hat{e}_3 - H_1\hat{e}_1 - H_2\hat{e}_2 \tag{11}$$

Using Eqs. (9) and (10), substituting $\hat{n}$ and $\hat{t}$ in Eq. (11), we get:

$$\begin{aligned} T &= Vsin\alpha + H_1 cos\alpha \\ N &= \sqrt{\bar{N}^2 + H_2^2} \\ \hat{n} &= \frac{\bar{N}}{N} sin\alpha\hat{e}_1 - \frac{H_2}{N}\hat{e}_2 + \frac{\bar{N}}{N} cos\alpha\hat{e}_3 \end{aligned} \tag{12}$$

where $\bar{N} = V cos\alpha - H_1 sin\alpha$.

Further, the incremental horizontal and vertical displacements can also be resolved along normal and tangential directions. However, the incremental displacements δh_1 and δh_2 are associated with the base particle, and incremental displacement δv is associated with the top particle. To obtain the relative displacement of the two particles, the incremental displacement vector must be written in the reference frame of one of the particles. For the following, the top particle is chosen as reference, such that the base particle undergoes an incremental displacement of $\delta h_1\hat{e}_1 + \delta h_2\hat{e}_2 - \delta v\hat{e}_3$. This incremental displacement vector is resolved along $\hat{t}^1 = \hat{t}$, $\hat{t}^2 = \hat{n} \times \hat{t} = \frac{H_2}{N} sin\alpha\hat{e}_1 + \frac{\bar{N}}{N}\hat{e}_2 + \frac{H_2}{N} cos\alpha\hat{e}_3$, and $\hat{n}$:

$$\begin{aligned} \begin{Bmatrix} \delta t_1 \\ \delta t_2 \\ \delta n \end{Bmatrix} &= \begin{bmatrix} t_1^1 & t_2^1 & t_3^1 \\ t_1^2 & t_2^2 & t_3^2 \\ n_1 & n_2 & n_3 \end{bmatrix} \begin{Bmatrix} \delta h_1 \\ \delta h_2 \\ -\delta v \end{Bmatrix} \\ \delta t_1 &= \delta h_1 cos\alpha + \delta v sin\alpha \\ \delta t_2 &= \frac{H_2}{N}(\delta h_1 sin\alpha - \delta v cos\alpha) + \frac{\bar{N}}{N}\delta h_2 = 0 \\ \delta n &= \frac{\bar{N}}{N}(\delta h_1 sin\alpha - \delta v cos\alpha) - \frac{H_2}{N}\delta h_2 = 0 \end{aligned} \tag{13}$$

The tangential displacement can be calculated by taking cumulative sums of δt_1. Also, note that the incremental normal deformation at contact is assumed to be zero during sliding (in fact, this assumption helps us in estimating the contact tangent along the direction of sliding). This assumption holds only if the normal load and stiffness remain constant during sliding. The tests where vertical load is increased during sliding should be discouraged, as the increase in vertical load may bring extra normal deformation, which is not accounted for, making the orientation of contact inaccessible as δn is no longer zero.

5. Discussion

It is likely that the data obtained from particle-particle contact tests will hold a significant importance in the

development or validation of new contact models (Altuhafi et al., 2024) for discrete element simulations and understanding of contact behaviour. The previous sections present a set of precautions and procedures that must be followed while carrying out these experiments, along with the care needed in the analysis of the results. With such measures, the understanding of particle–particle contact behaviour can be studied with a good degree of accuracy. An example is discussed here with vertical and tangential shearing stages on Leighton Buzzard sand. The particles are aligned apex to apex, as shown in Fig. 13a, to have a known orientation of contact in the vertical loading stage. Despite the assurance from the digital microscope (inter-particle camera) images, the contact plane may be inclined with the horizontal plane locally. For estimation of the normal load and normal displacement (Fig. 13a), it is assumed that the friction either does not mobilise or mobilises insignificantly in vertical loading. After vertical loading, the particles are sheared horizontally. The contact tangent in the h_1-v plane is estimated using Eq. (4) and the h_1-v profile (Fig. 13b). Forces and displacements are resolved using Eqs. (12) and (13) and are plotted in Fig. 13c. In Fig. 13c, the blue axes and line represent T/N (force ratio after corrections) and tangential displacement, while the orange axes and line represent H_1/V (force ratio of recorded loads). The effect of local slope correction is clearly visible in Fig. 13c; H_1/V shows a range of friction values, while T/N stabilises after sliding. The tangential displacement and forces also lead to a correct estimation of tangential stiffness (shown in Fig. 13d) instead of relying on the horizontal displacement. To illustrate further the efficacy of the topography correction, two additional sets of experiments were performed. Fig. 14 present T/N vs tangential displacement for two different pairs of particles of

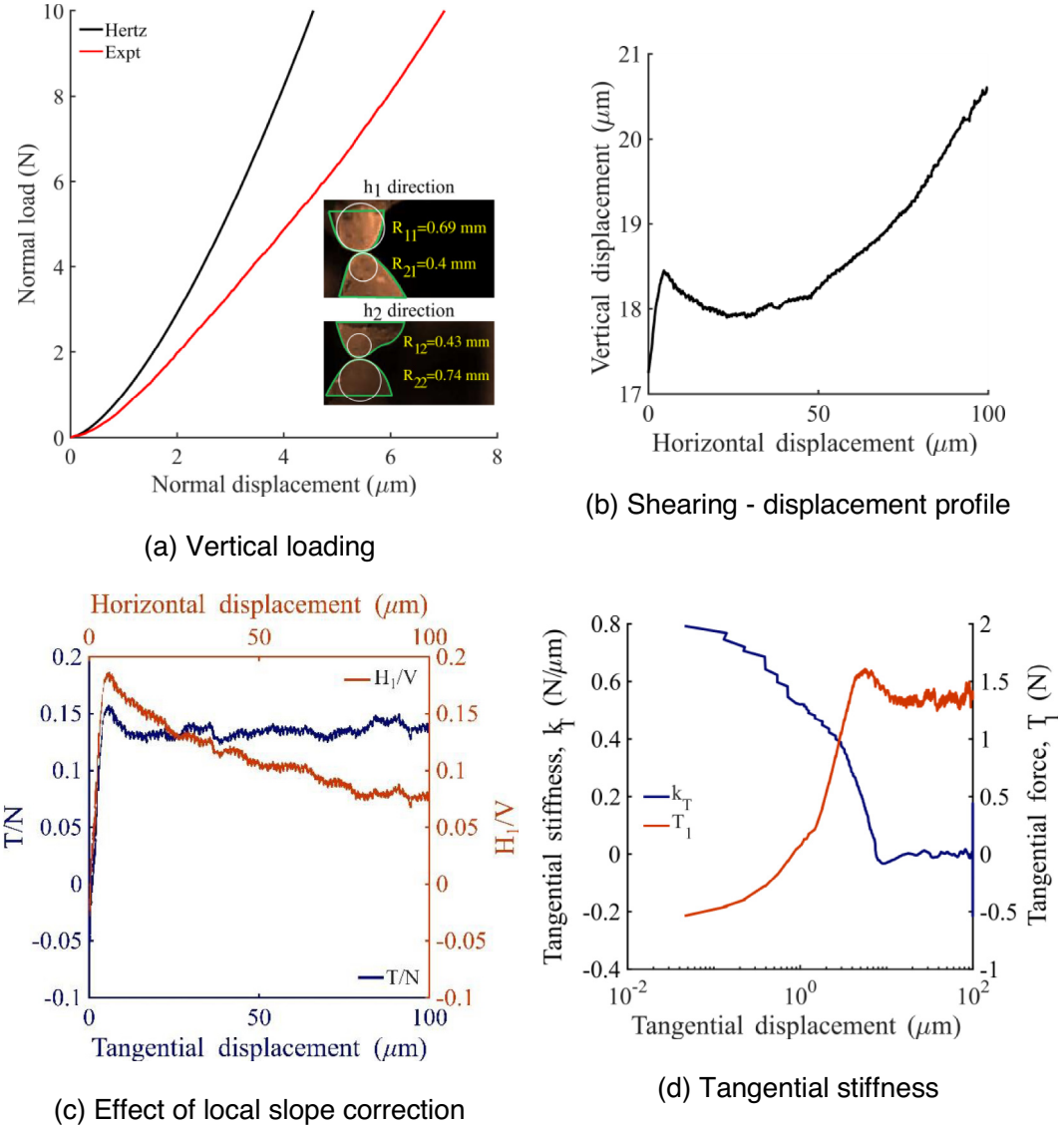

Fig. 13. An example test on Leighton Buzzard Sand. (a) vertical loading, (b) displacement profile during shearing, (c) effect of local slope correction, (d) tangential stiffness with tangential displacement.

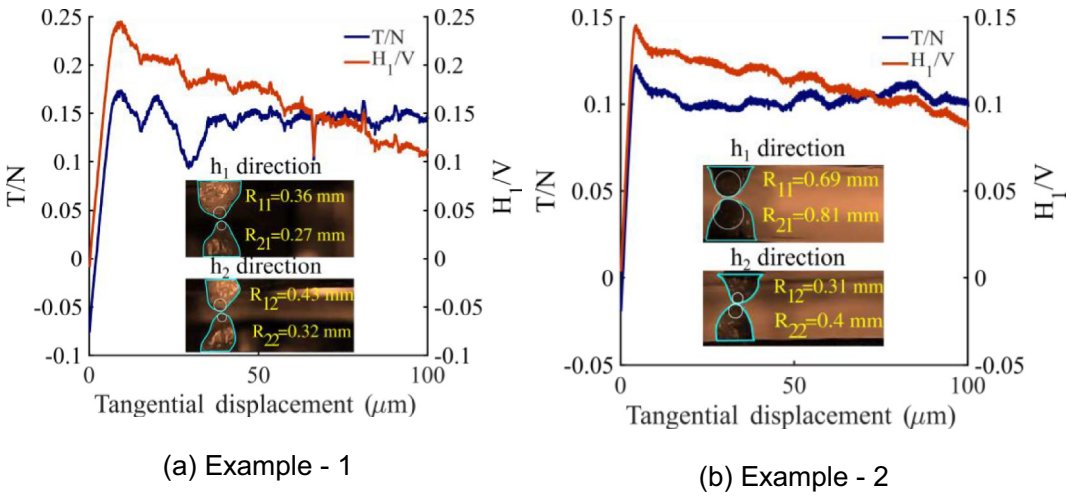

Fig. 14. Examples of inter-particle tests on Leighton Buzzard Sand demonstrating the efficacy of proposed topography correction. (a) Example 1 with normal load of 5 N, (b) Example 2 with normal load of 15 N.

different shape complexity. Despite the varying complexity of shape profiles, μ is nearly the same for both set of particles in Fig. 14a and b. As discussed earlier, the moments generated from the nonalignment of the vertical and horizontal loads with the point of contact would cause a non-uniform distribution of normal and tangential traction on the contact region, along with errors in the functioning of the load cells. For any design of inter-particle apparatus, it should be the top priority to have the contact point or region pass through the axes of loading. The fixture used for setting of particle on the platens, shown in Fig. 8, ensures the centring of the particle peak on the platen, in turn leading to alignment with the vertical load. For alignment with horizontal axes, particles should be ground to a uniform prefixed height, and if that is not possible, spacers underneath the base platens can be used to adjust the height. If the compliance tests are done with a certain type of glue, for all the tests, only that type of glue must be used, as changing the glue may change the horizontal or vertical compliance.

Natural granular particles bring a significant degree of complexity in studying them. Despite the above measures, there are certain sands, such as coral sands or other crushable materials, that present a significant difficulty in conducting the experiments and acquiring good-quality data. Such particles are very difficult to grind flat, as they are much easier to crush than to grind. In vertical loading, if a desired load has to be reached, these particles should be tested in load control after establishing the contact, as breakage events may cause repeated loss of contact. The tangential shearing of crushable particles is often accompanied by excessive breakage; hence, it becomes very challenging to estimate the orientation of the contact from the h_1-v profile. This makes an accurate assessment of normal and tangential load very difficult. A simple and approximate alternative may be used in this case by continuously capturing the particle–particle contact through the digital microscopes. The contact orientation can be estimated using the slope of the contact tangents in the images. It should be noted that this solution would not work if the contact is not visible due to the complex topography of particles.

In the coming years, there may be many more alternative apparatuses and loading conditions to test the particle–particle contact behaviour. This article provides a set of cautions that should be used in designing the apparatus and the loading conditions so as to obtain accurate contact behaviour of naturally complex particulate geomaterials.

6. Conclusions

This study aimed to provide detailed guidance for designing and performing inter-particle tests and their analysis to help with the development of contact models for irregular particles. It also serves as a standardisation of experimental procedures, ensuring more robust results.

The error in the measurement of forces and displacements in inter-particle tests is a function of apparatus compliance, sled friction, and resolution of transducers and sensors. Keeping this in mind, a detailed procedure for apparatus calibration is provided that must be done frequently. Furthermore, the article also details a standardised procedure to perform the particle–particle experiments, starting with preparation before the experiment, establishing contact and different loading stages. Various loading and displacement rates are provided along with their justifications for quasi-static loading.

The unknown profile of particles near their contact was a major challenge in obtaining the orientation of the contact plane and resolving forces. The article derives the equations to obtain the accurate contact plane in sliding while recommending apex-apex contact in vertical loading.

With the known contact orientation, a derivation of the true tangential and normal forces and displacements is provided along with the equations in terms of vertical and horizontal forces and displacements. These lead to an accurate assessment of the contact normal and tangential stiffness, along with the coefficient of friction.

The recommendations and findings of this article will improve the quality of particle–particle experiments and contribute to exploring, accurately, the physics of sands, ballasts, rockfill, and other coarse-grained irregular geomaterials.

CRediT authorship contribution statement

Saurabh Singh: Writing – review & editing, Writing – original draft, Validation, Software, Methodology, Formal analysis, Data curation, Conceptualization. **Matthew Richard Coop:** Writing – review & editing, Supervision, Software, Resources, Project administration, Methodology, Conceptualization. **Beatrice Anne Baudet:** Writing – review & editing, Supervision, Resources, Project administration, Funding acquisition.

Acknowledgements

The authors are grateful for the technical support of Mr. Matthew Wilkinson, Mr. Charlie Laybourn Waller, and Mr. Les Irwin in our research, and to Dr. Pedro Ferreira for providing useful solutions to resolve the electronic problems with the inter-particle apparatus. The work was wholly funded by the EPSRC Project No. EP/W000563/1.

Appendix A. Calibration of sensors

Fig. A.1 shows the custom-made setups designed for the calibration of load cells and displacement transducers. Fig. A.1a shows the calibration setup of miniature load cells. The load cells are screwed onto a custom-made base and top platform, and then standard (calibrated) loads are applied to measure the voltage produced by the load cell (through an amplifier). A typical calibration of load cells is presented in Fig. A.1b. Note that the calibration coefficient of the horizontal load cells is double that of the vertical load cell. This reflects that the vertical load cell is double the capacity of the horizontal load cell. These load cell capacities were chosen as the coefficient of friction for natural granular materials is often less than 0.5. For the calibration of displacement transducers, a calibration stage was used as shown in Fig. A.1c. The calibration stage has a fixture to hold the transducer firmly and a micrometre attached to a target metallic plate. The transducer is kept in proximity with the target, and the micrometre is rotated to move the target relative to the transducer. The voltage corresponding to different micrometre displacements is recorded and plotted for calibration (as shown in Fig. A.1d). The calibration coefficients for all three transducers are similar.

For cyclic and time-dependent loading, creep or relaxation and hysteresis of sensors should also be calibrated. This is to confirm whether the hysteresis or relaxation observed in the contact behaviour is really due to the sand or has its origin in the sensor. Fig. A.2a shows the hysteresis in the load cells, which is negligible. Furthermore, no electronic drift or creep was observed in the load cells, as shown in Fig. A.2b.

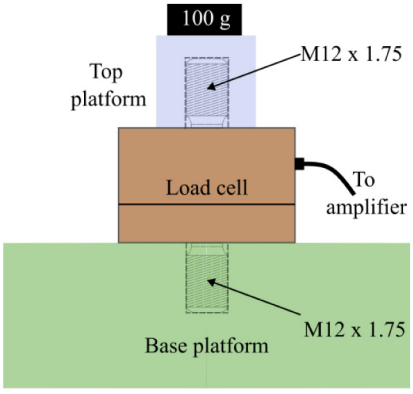

(a) calibration setup for the load cell

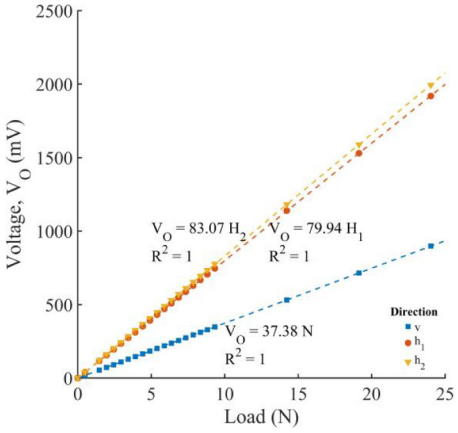

(b) calibration of load cells

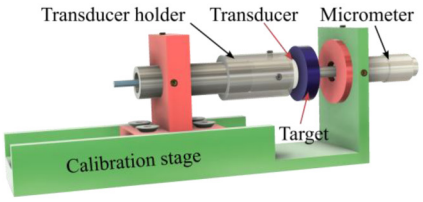

(c) calibration setup for displacement transducer

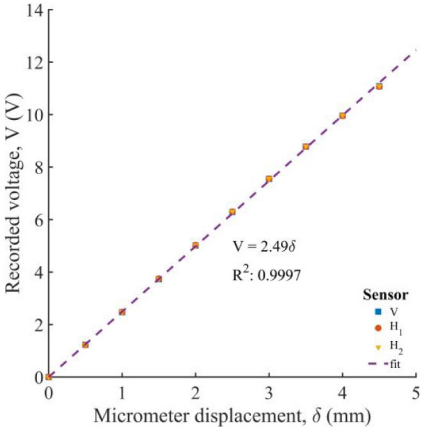

(d) calibration of displacement transducers

Fig. A.1. Calibration of load cells and displacement transducers. (a) calibration setup for load cells; (b) calibration of load cells; (c) calibration setup for displacement transducers; (d) calibration of displacement transducers.

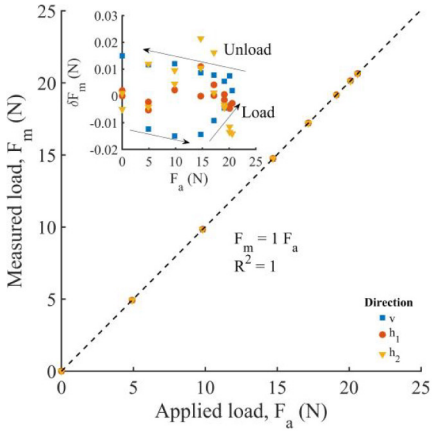

(a) Hysteresis in load cells with unload-reload

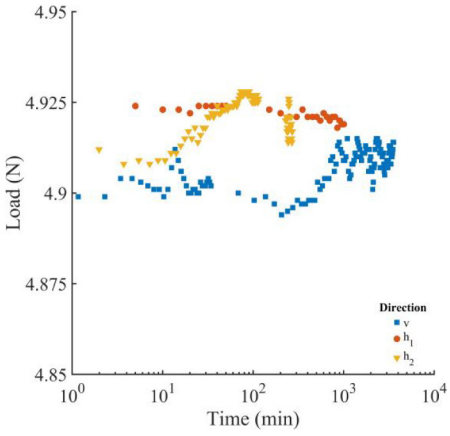

(b) Creep in load cells

Fig. A.2. Performance of the load cell with time-dependent loading. (a) hysteresis in load cells during load-unload cycle; (b) Electronic drift and creep in load cells with time at a constant load.

Appendix B. Supplementary material

Supplementary material, a set of movies illustrating the relative motion of particles in the inter-particle apparatus, can be found online at https://doi.org/10.1016/j.sandf.2026.101807.

References

Altuhafi, F., Baudet, B.A., Coop, M.R., 2024. An investigation of the applicability of contact models to the normal load-deformation behaviour of artificially shaped granite. Acta Geotech. 19 (6), 3447–3465.

Barrett, P.J., 1980. The shape of rock particles, a critical review. Sedimentology 27 (3), 291–303.

Boulanger, J., 1992. The "Motifs" method: an interesting complement to ISO parameters for some functional problems. Int. J. Mach. Tool Manuf. 32 (1–2), 203–209.

Cavarretta, I., Rocchi, I., Coop, M.R., 2011. A new interparticle friction apparatus for granular materials. Can. Geotech. J. 48 (12), 1829–1840.

Cheng, H., Shuku, T., Thoeni, K., Yamamoto, H., 2018. Probabilistic calibration of discrete element simulations using the sequential quasi-Monte Carlo filter. Granul. Matter 20 (1), 11.

Cole, D.M., Mathisen, L.U., Hopkins, M.A., Knapp, B.R., 2010. Normal and sliding contact experiments on gneiss. Granul. Matter 12 (1), 69–86.

Cundall, P.A., Strack, O.D., 1979. A discrete numerical model for granular assemblies. Geotechnique 29 (1), 47–65.

Dafalias, Y.F., Manzari, M.T., 2004. Simple plasticity sand model accounting for fabric change effects. J. Eng. Mech. 130 (6), 622–634.

Hertz, H., 1881. Über die Berührung fester elastischer Körper. J. Reine Und Angewandte Mathematik 92, 156.

Iwashita, K., Oda, M., 1998. Rolling resistance at contacts in simulation of shear band development by DEM. J. Eng. Mech. 124 (3), 285–292.

Li, Y., Otsubo, M., Kuwano, R., Nadimi, S., 2021. Quantitative evaluation of surface roughness for granular materials using Gaussian filter method. Powder Technol. 388, 251–260.

Mirghasemi, A.A., Rothenburg, L., Matyas, E.L., 1997. Numerical simulations of assemblies of two-dimensional polygon-shaped particles and effects of confining pressure on shear strength. Soils Found. 37 (3), 43–52.

Nardelli, V., Coop, M.R., 2019. The experimental contact behaviour of natural sands: normal and tangential loading. Géotechnique 69 (8), 672–686.

Nardelli, V., 2017. An experimental investigation of the micromechanical contact behavior of soils PhD thesis. Architechture and Civil Engineering Department, City University of Hong Kong, Hong Kong, China.

Nguyen, D., Chen, Y., Martinez, A., 2025. A DEM sensitivity study on the effects of contact parameters on triaxial response for the development of a calibration method. Comput. Geotech. 184 107241.

Otsubo, M., O'Sullivan, C., 2018. Experimental and DEM assessment of the stress-dependency of surface roughness effects on shear modulus. Soils Found. 58 (3), 602–614.

Persson, B.N., Albohr, O., Tartaglino, U., Volokitin, A.I., Tosatti, E., 2004. On the nature of surface roughness with application to contact mechanics, sealing, rubberfriction and adhesion. J. Phys. Condens. Matter 17 (1), R1.

Roscoe, K.H., Schofield, A., Thurairajah, A., 1963. Yielding of clays in states wetter than critical. Geotechnique 13 (3), 211–240.

Roscoe, K.H., Schofield, A.N., Wroth, A.P., 1958. On the yielding of soils. Geotechnique 8 (1), 22–53.

Sandeep, C.S., Todisco, M.C., Nardelli, V., Senetakis, K., Coop, M.R., Lourenco, S.D.N., 2018. A micromechanical experimental study of highly/completely decomposed tuff granules. Acta Geotech. 13 (6), 1355–1367.

Santamarina, C., Cascante, G., 1998. Effect of surface roughness on wave propagation parameters. Géotechnique 48 (1), 129–136.

Senetakis, K., Coop, M., 2014. The development of a new micro-mechanical inter-particle loading apparatus. Geotech. Test. J. 37 (6), 1028–1039.

Senetakis, K., Coop, M.R., 2015. Micro-mechanical experimental investigation of grain-to-grain sliding stiffness of quartz minerals. Exp. Mech. 55 (6), 1187–1190.

Senetakis, K., Coop, M.R., Todisco, M.C., 2013. The inter-particle coefficient of friction at the contacts of Leighton Buzzard sand quartz minerals. Soils Found. 53 (5), 746–755.

Shin, H., Santamarina, J.C., 2013. Role of particle angularity on the mechanical behavior of granular mixtures. J. Geotech. Geoenviron. Eng. 139 (2), 353–355.

Singh, S., Baudet, B.A., Coop, M.R., 2025. Correction for particle surface topography in inter-particle tangential shearing tests. In: IOP Conference Series: Earth and Environmental Science, vol. 1480(1). IOP Publishing.

Skinner, A.E., 1969. A note on the influence of interparticle friction on the shearing strength of a random assembly of spherical particles. Geotechnique 19 (1), 150–157.

Sun, Q., Zheng, J., 2020. Clone granular soils with mixed particle morphological characteristics by integrating spherical harmonics with Gaussian mixture model, expectation–maximization, and Dirichlet process. Acta Geotech. 15 (10), 2779–2796.

Verdugo, R., Ishihara, K., 1996. The steady state of sandy soils. Soils Found. 36 (2), 81–91.

Wadell, H., 1932. Volume, shape, and roundness of rock particles. J. Geol. 40 (5), 443–451.

Wong, C.P., Coop, M.R., 2023. The contact mechanics of a UK railway ballast. Géotechnique 74 (13), 1700–1712.

Wong, C.P., 2022. Micro-mechanical contact behaviour for railway ballast PhD thesis. University College London.

Yang, H., Baudet, B.A., Yao, T., 2016. Characterization of the surface roughness of sand particles using an advanced fractal approach. Proc. R. Soc. A: Math. Phys. Eng. Sci. 472 (2194) 20160524.

Zhao, J., Zhao, S., Luding, S., 2023. The role of particle shape in computational modelling of granular matter. Nat. Rev. Phys. 5 (9), 505–525.

Zheng, J., Hryciw, R.D., 2015. Traditional soil particle sphericity, roundness and surface roughness by computational geometry. Géotechnique 65 (6), 494–506.